

Hourglass SiO₂ coating increases the performance of planar patch-clamp.

Thomas Sordel, Stéphanie Garnier-Raveaud, Fabien Sauter, Catherine Pudda, Frédérique Marcel, Michel de Waard, Christophe Arnoult, Michel Vivaudou, François Chatelain, Nathalie Picollet-d'Hahan

► **To cite this version:**

Thomas Sordel, Stéphanie Garnier-Raveaud, Fabien Sauter, Catherine Pudda, Frédérique Marcel, et al.. Hourglass SiO₂ coating increases the performance of planar patch-clamp.. Journal of Biotechnology, Elsevier, 2006, 125 (1), pp.142-54. 10.1016/j.jbiotec.2006.02.008 . inserm-00381712

HAL Id: inserm-00381712

<https://www.hal.inserm.fr/inserm-00381712>

Submitted on 10 Jun 2009

HAL is a multi-disciplinary open access archive for the deposit and dissemination of scientific research documents, whether they are published or not. The documents may come from teaching and research institutions in France or abroad, or from public or private research centers.

L'archive ouverte pluridisciplinaire **HAL**, est destinée au dépôt et à la diffusion de documents scientifiques de niveau recherche, publiés ou non, émanant des établissements d'enseignement et de recherche français ou étrangers, des laboratoires publics ou privés.

Hour-glass SiO₂ coating increases the performance of planar patch-clamping

Thomas Sordel^{*,#}, Stéphanie Garnier-Raveaud^{*,#}, Fabien Sauter[§], Catherine Pudda[§], Anne Simon^{*}, Michel De Waard[^], Christophe Arnoult[^], Michel Vivaudou[°], François Chatelain^{*}, Nathalie Picollet-D'hahan^{*,¶}.

^{*} BioChip Laboratory - CEA, 17 rue des Martyrs, 38054 Grenoble cedex 9, France

[^] Laboratoire Canaux Calciques, Fonctions et Pathologies, INSERM U607, CEA Grenoble, France

[°] Laboratoire Biophysique Moléculaire et Cellulaire, CEA Grenoble, France

[§] LETI – CEA Grenoble, France

[#] These authors equally contributed to this work.

[¶] Correspondence should be addressed to N.P-D. (picolletdhahan@dsvsud.cea.fr)

ABSTRACT

Obtaining high-throughput electrophysiology recordings is an ongoing challenge in fundamental ion channel biophysics and drug discovery. One particular area of development is the replacement of glass pipettes with planar devices in order to increase the throughput. However, successful patch-clamp recording depends on an ideal surface coating that promotes and stabilizes giga-seals formation. Here, we describe a method for designing chips that are suitable for planar patch-clamping. The method was based on a correlation study taking into account dimension and size of the pores, surface roughness and chip capacitance. The influence of these parameters on the quality of the seal was then assessed. Plasma-enhanced chemical vapour deposition (PECVD) of SiO₂ led to a tighter seal and resistance than a flat, thermal SiO₂ surface. The performance of PECVD chips was validated assessing BK(Ca) and low conductance IRK1 potassium channels and endogenous cationic currents recordings from CHO and HEK-293 cells. We assume that the systematic investigation of chip parameters to improve seal quality will result in the production of reliable chips for planar patch-clamp applications allowing electrophysiological recordings from a wide range of cell lines, primary cultures and isolated native cells.

Keywords: planar patch-clamp, BK(Ca) channels, IRK1 channels, PECVD coating, AFM, SEM.

INTRODUCTION

Ion channels represent a large family of potential drug targets (Venter et al., 2001, Wang and Li, 2003), and have thus become important objects in the drug discovery/screening process. However, the lack of high-throughput assays has hampered their use for screening purposes and still constitutes a bottleneck in lead optimization steps (Xu et al., 2004, Wood et al., 2004). Since 1998, efforts have been made to automate electrophysiology (Xu et al., 2004) and several important technological advances have been made. To increase the throughput of patch-clamp recordings, attempts have been made to replace the traditional pipette with a planar substrate. Glass was the first material used for planar patch-clamp recording because this material has good dielectric properties and interacts well with membrane lipids (Fertig et al., 2003). Nevertheless, microstructuring processes involving glass are complex and require specific equipments. A wide range of other materials, and sometimes a hybrid assembly of different materials, have been also tested : PDMS (Sigworth and Klemic, 2002), SiO₂ coated plastic chips (Wang and Li, 2003), SiO₂ coated silicon chips (Asmild et al., 2003), quartz (Stett et al., 2003b) and encapsulated silicon chips in a plastic matrix (Seo et al., 2004). Nevertheless, stable high-resistance seals (giga-seals) are still elusive. The success rates on the “best” materials remain low, ranging between 30 and 50%, depending on the cell type (Stett et al., 2003a, Owen and Silverthorne, 2002). The optimum choice of suitable material and surface coatings has yet to be defined (Xu et al., 2003) because of the complex nature of the seal. Even under optimal conditions, seal resistance values remained consistently below the minimum that is required for highly resolved currents and single channel analysis. Therefore, high-throughput screening for agonists or antagonists of ion channels using planar substrates is mainly done in surrogate cell systems in which the channel of interest is stably or transiently overexpressed (Chien, 2003).

The optimisation of planar patch-clamp cell sealing involves both biological and technological approaches. Some authors introduced new procedures in order to improve the quality of the cell

suspension (Bruggemann et al., 2003) or optimize the identification of cells that are suitable for patch-clamping (Mc Dowell and Gray, 2004).

Here, we describe a method that is based on the modification and characterization of the dimension and shape of the pores, surface roughness and chip capacitance in relation to the quality of the seal. We have focused on silicon-based chips coated with a SiO₂ layer, the production of which offers high accuracy and flexibility of microstructuration and surface functionalisation. This approach has led to a model of PECVD SiO₂ coating defining an “hourglass” shape of the hole (Fig. 2). We demonstrate that by decreasing the size of the microhole and modifying shape and roughness, the seal resistance in comparison to flat thermal SiO₂ treatment was enhanced. Secondly, decreasing chip capacitance allowed ion channels of low conductance and endogenous channel activities to be recorded in a whole-cell configuration mode. Two transfected cell lines (CHO and HEK-293) displayed the electrophysiological signatures of the expected BK(Ca) and IRK1 potassium channel activities and those of cationic endogenous channels. (nomenclature officielle: BK(Ca) = K_{Ca}1.1)

Our approach relies on a growing database of experimental correlations allowing the optimization of chip design to potentially shift from whole cell to highly resolved unitary currents recordings and from recombinant to native channel studies. We show here that the planar interface can be adapted to specific cell types by modifying and controlling the features of the chip, thus greatly expanding the application options to a wide range of different cell lines, primary cultures and isolated native cells.

MATERIAL AND METHODS

Device assembly

The patch-on-a-chip device was described previously (Picollet-D'Hahan et al., 2004). The chip consists of 9 independent cell-patch sites, each defined by a couple of o-rings (Inner diameter I.D. = 3 mm, Outer diameter O.D. = 5 mm) which act as walls of individual chambers. The so-defined top and bottom

compartments communicate through a hole of 2.5 μm diameter in a 2.12 μm thick silica membrane. The compartments are connected to a network of microfluidic capillaries, allowing solutions to be supplied and exchanged independently. Two printed circuit boards (PCB) with 9 Ag/AgCl planar electrodes were assembled in a “sandwich” manner and connected to a patch-clamp amplifier.

Chip passivation

Two types of chips were studied: chips coated with a SiO_2 layer grown with a thermal oxidation (thermal SiO_2) and chips with an additional PECVD SiO_2 layer on the upper side. The fabrication process of the chips was described previously (Picollet-D'Hahan et al., 2004). PECVD was deposited at 300°C with a rate of 1300 $\text{\AA}/\text{min}$. This resulted in a layer with a thickness of 0.5 μm to 1.5 μm . Three PECVD SiO_2 layer thicknesses were investigated (Table 1) and studied in terms of chip resistance and capacitance values.

Atomic Force Microscopy measurements

Atomic Force Microscopy (AFM) experiments were performed with a DimensionTM 3100 AFM (Digital Instruments, Santa Barbara, CA) and a Nanoscope IV controller (Digital Instruments) equipped with a large-range scanner (maximum XY scan range of 90 μm x 90 μm with vertical Z range of 6 μm). Measurements were obtained in the AFM contact mode by using silicon nitride cantilevers with a 0.12 N/m nominal spring constant, and a scanning velocity of 30 – 180 $\mu\text{m}/\text{s}$. Images were recorded in the constant force mode with minimal external force.

Cell preparation

Human Embryonic Kidney 293 (HEK-293) cells were stably transfected with pcDNA3.1-HA-mBKc (Creacell, La Tronche, France), a plasmid construct carrying the coding sequence of mBKc (mSlo A48206). The cells were cultured in Dulbecco's modified Eagle's medium supplemented with 10% (V/V)

foetal calf serum, 1.2 mg/ml geneticin, 1% penicillin-streptomycin and 1% L-glutamine in flasks. Chinese Hamster Ovary (CHO) cells were stably transfected with pcDNA3.1-HA-mIRK1 (Creacell), a plasmid carrying the coding sequence of the IRK1 protein. The cells were cultured in Ham F12 medium supplemented with 10% (V/V) foetal calf serum, 1.2 mg/ml geneticin, 1% penicillin-streptomycin and 1% L-glutamine in flasks.

Cells were pre-washed with Phosphate Buffered Saline (PBS, Invitrogen, Cergy-Pontoise, France). To detach the cells prior to the experiment, Accutase, rather than trypsin/EDTA, proved to be most effective (Tao et al., 2004). Accutase-isolated cells revealed better membrane integrity and optimised morphology. In addition, this enzyme has been reported to not alter ion channel functionality. The number of aggregates was reduced and the suspension more homogeneous, something that is particularly important in order to exclusively immobilize one individualized cell onto the microhole. After detachment, cells were centrifuged at 360 x g and resuspended in a mixture of PBS/Accumax at a concentration of 2.10^5 cells/ml and kept at 4°C under agitation. Immediately prior to the planar patch-clamp experiments, the cells were concentrated in electrophysiological solution to 5.10^5 cells/ml.

Electrophysiology

Experimental conditions were similar to those used in conventional patch-clamp experiments, where the “bath” solution becomes the upper chamber solution and the intrapipette solution the lower chamber solution. The upper chamber solution contained (in mM): 118 NaCl, 5.6 KCl, 2.4 CaCl₂, 1.2 MgCl₂, 10 HEPES, 11 glucose, pH 7.4 (with NaOH), conductivity 1.32 S/m. In inhibition experiments, BaCl₂ and iberiotoxin (Sigma, St Quentin Fallavier, France) were added. The lower chamber contained (in mM): 30 KCl, 110 K-aspartate, 1 MgCl₂, 0.1 CaCl₂, 1 EGTA, 10 HEPES, pH 7.3 (with KOH), conductivity 1.17 S/m. Experiments were conducted at room temperature (20°C) and cells were studied in the whole-cell mode. For each experiment, one microhole out of 9 was examined as followed: the bottom chamber of the device was filled with the solution first, followed by the upper chamber. Care was taken to eliminate

bubbles in the fluidic circuit. Microhole resistance (R_h) was monitored by applying a square wave of voltage (5 mV amplitude and 10 ms duration) across the microfluidic chambers through the microhole with Ag/AgCl electrodes. The cellular suspension was then injected into the upper chamber (~2,500 cells/chamber) and a negative pressure of -100 mbar to -200 mbar was applied to the lower chamber in order to attract one cell onto the microhole while simultaneously monitoring patch resistance. This phase of the process is successfully completed within 30 seconds to get one cell onto the microhole. A suction was then maintained until a seal was established. Then the negative pressure could be released. Whole-cell configuration was obtained by applying a 1 V pulse during 100 μ s to snap the isolated membrane patch. Subsequently, voltage control and current recordings from the cell membrane were performed. Acquisition was performed with the Multiclamp 700A amplifier (Axon Instruments, Union City, USA). All traces were sampled at 20 kHz and filtered at 2 kHz. The current-voltage (I-V) relationships were obtained from voltage ramps from 0 mV to +120 mV with 10 mV increments over 400 ms for BK(Ca) channels, and from +60 mV to -120 mV with 10 mV decrement during 200 ms for IRK1 channels.

RESULTS

High-resistance seals were previously obtained with non-transfected Jurkat cells on 2.5 μ m diameter holes structured in a 2 μ m thick silica membrane (Piccollet-D'Hahan et al., 2004). However, seal resistances depended very much, as was expected, on the type of cells used. In addition, the seals did not prove to be tight enough for whole-cell mode measurements of transfected CHO cells. Thus, we explored novel ways to modify cell patch-site parameters such as microhole size and surface properties. Hydrophilic surfaces were previously shown to promote the attachment of hydrophilic cell membranes (Corey and Stevens, 1983). In order to test whether the seal was sufficiently tight for use on cells expressing ion channels, the chip surface was passivated with SiO₂ PECVD leading to a more hydrophilic surface. In addition, the PECVD coating was expected to reduce the microhole diameter to less than 2.5 μ m and so lead to higher hole resistance values and possibly higher seal resistance values. Chips with a thermal SiO₂ surface layer

and chips with an additional PECVD SiO₂ layer on the upper side were used to assess the effect of the additional PECVD layer on the performance of the chip in terms of pore dimension, pore shape, surface roughness, chip capacitance and then weighed against seal quality.

PECVD SiO₂ coating alters the physical properties of microholes

Both thermal and PECVD SiO₂ coated chips were observed by electron microscopy in order to determine microhole size and shape. On thermal SiO₂ chips, the nominal microhole diameter of 2.5 μm showed a well-defined round circle (Fig. 1A). A 1.5 μm PECVD layer reduced the microhole diameter to 1.7 μm while introducing roughness around the aperture (Fig. 1B).

The influence of the passivation process on surface topography was analysed by AFM (atomic force microscopy). The thermal SiO₂ surface appeared extremely clean and homogeneous (Fig. 1C). In contrast, asperities and irregularities were present on the PECVD SiO₂ surface (Fig. 1D). Some roughness was determined on either side in a zone of 7 μm diameter around the microhole and divided into 4 areas (Fig. 1C,D). The arithmetic average of the absolute values of the surface height deviations (measured from the mean plane) was calculated for each area, with a value of 2.4 ± 0.1 nm (n=4) on thermal SiO₂ surfaces and 9.0 ± 1.4 nm (n=4) on PECVD SiO₂ surfaces. Flatness in the immediate vicinity of the microhole was quantified and showed a crown measuring 45 nm in height and a width of 800 nm on the PECVD SiO₂ surface (Fig. 1D,F).

Modelling of patch-site resistance and capacitance

Reproducibility and accuracy of the SiO₂ PECVD process were evaluated by measuring the microhole resistance R_h of each chip for the different thicknesses of the PECVD SiO₂ layer: 0, 0.5, 1 and 1.5 μm. R_h , which is an indirect measure of microhole diameter, was determined for a device that contained an intrapipette saline solution but no cells. The results showed a clear correlation between resistance and diameter (Table 1). Typically, the mean experimental resistance for a 2.5 μm diameter aperture was 0.55

$\pm 0.1 \text{ M}\Omega$ and increased to $1.15 \pm 0.1 \text{ M}\Omega$ with a $1.5 \text{ }\mu\text{m}$ SiO_2 layer. In order to further investigate the influence of PECVD SiO_2 deposition on Rh, two models were developed to study the importance of the microhole shape. System resistance can be modelled by only taking into account the cell-patch site resistance (Matthews and Judy, 2003). The cell-patch site can be modelled as a conductor with a resistance that matched that of the intrapipette solution in the microhole (Fig. 2A). In model 1, it was assumed that the PECVD deposition led to a cylindrical shape of the aperture (Fig. 2B). Theoretical values reported in Fig. 2D were calculated using Eq. 1 giving the resistance for a cylindrical shape as a function of electrolyte resistance ρ , hole height l and surface S of the aperture :

$$R_h = \rho \frac{l}{S} \quad \text{Eq. 1}$$

Fig. 2D shows that the theoretical microhole resistance values which were calculated on the basis of a cylindrical shape are higher than the experimental values.

In model 2, which is based on Scanning Electron Microscopy (SEM) observations (Fig. 1B), it was assumed that PECVD deposition led to an "hourglass" shaped hole. It was expected that holes would have the axial symmetry depicted in Fig. 2C and an ellipsoidal curve was used to model the shape of holes. The equation allowing the determination of the microhole diameter as a function of the height z is:

$$\phi = \phi_0 - (\phi_0 - \phi_d) \left[1 - \left(\frac{2z}{e_d + e_0} \right)^2 \right]^{\frac{1}{2}} \quad \text{Eq. 2}$$

with the initial microhole diameter $\phi_0 = 2.5 \text{ }\mu\text{m}$, the measured microhole diameter ϕ_d after PECVD deposition, the thermal SiO_2 thickness e_0 and the deposit thickness e_d . Eq. 1 was discretized (Ca veut dire???) on the total height $(e_d + e_0)$ in order to calculate theoretical resistances. Fig. 2D and Table 1 show good agreement between the average resistance of four different cell-patch-site diameters and the modelled cell-patch site resistance.

In our device (Fig. 2A), the Si-based structure leads to a high capacitance since it functions as a capacitor between the electrophysiological medium of the upper (*zone A*) and lower (*zone D*) chambers and the isolating SiO₂ layers (*zone B divided in B₁ and B₂*) on either side of the silicon layer (*zone C*). The model for the capacitance is provided by Eq. 3 where C_{PS} stands for the total capacitance of the cell-patch site, C_{AD} and C_{AC} for the front and C_{CD} for the back capacitances.

$$C_{PS} = C_{AD} + \left(\frac{1}{C_{AC}} + \frac{1}{C_{CD}} \right)^{-1} \quad \text{Eq. 3}$$

$$C = \epsilon_0 \epsilon_r \frac{S}{d} \quad \text{Eq. 4}$$

The capacitances reported in Table 1 were calculated using Eq. 3 and 4, with the insulating layer dielectric constant ϵ_r (4.5 for SiO₂), the surface S of the surrounding fluid, and the layer thickness d. In our configuration, C_{AD} can be ignored because the surface of the microhole SiO₂ membrane was only 0.004 mm² compared to the 7 mm² taken into account for the C_{AC} and C_{CD} contributions.

As expected, the cell-patch site capacitance, measured with a 263A potentiostat and a 1025 frequency response detector (Princeton Applied Research, Oak Ridge, USA) was reduced after PECVD passivation. Capacitance measurements performed before and after the positioning of a 1.5 μm PECVD layer showed a good correlation with theoretical results (Table 1).

PECVD SiO₂ coating improves seal frequency and quality

Chips with a thermal SiO₂ layer and chips with a 1.5 μm thick PECVD layer were experimentally characterized by evaluating seal values and cell membrane stability on the substrate whereas the two others intermediate PECVD thicknesses (0.5 and 1 μm) were used to study the evolution of microhole shape during the deposition process. Cell trapping and sealing were performed as described in the *Methods* section. The influence radius of suction through the microhole in which a cell is attracted was experimentally observed to be around 30-50 μm . Under this condition, cells in suspension within a

distance of 40 μm could be reliably positioned on the microhole and remained in this position even when the negative pressure was released. Immediately after trapping the cell, a negative pressure ranging from 0 mbar to -250 mbar was applied and the cell formed a seal on the patch aperture. The results indicate that PECVD SiO_2 passivation increased the seal success rate from nearly 0% (no seal higher than 100 $\text{M}\Omega$ on $n=30$ measurements without a PECVD layer) to 17% (15 seals higher than 100 $\text{M}\Omega$ on $n=90$ measurements with the PECVD layer). Taking into account all seals, the mean resistance of a cell on microhole varied from 30 $\text{M}\Omega$ without PECVD layer ($n=30$) to 155 $\text{M}\Omega$ ($n=90$) with PECVD layer. More precisely, with a PECVD layer, 9 seals out of 15 are set in a range of 100 $\text{M}\Omega$ to 200 $\text{M}\Omega$, 2 seals in a range of 200 to 500 $\text{M}\Omega$, 2 seals in a range of 500 to 1000 $\text{M}\Omega$ and 2 seals superior to 1 $\text{G}\Omega$ (Fig. 3). The highest seal resistance reached 7 $\text{G}\Omega$. 73% of the seals that were higher than 100 $\text{M}\Omega$ were lost within 2 minutes.

Low conductance and endogenous current recordings

Potassium currents were recorded without leak subtraction from HEK-293 cells stably expressing BK-type Ca^{2+} -activated channels. Current traces in Fig. 4A represent results from the execution of voltage command protocols with sweeps from 0 to +120 mV (by 10 mV increments) during 400 ms and demonstrate the effects of iberiotoxin (IBTX, 100 nM), a selective blocker of this channel type. Under these conditions, the outward currents were strongly inhibited by IBTX. The curves describing the current-voltage relationship, after leak current compensation, indicate an 88 % inhibition of BK(Ca) channels at +120 mV (Fig 4.B).

In order to test the setup with different cell lines and different types of channels, inward rectifier IRK1 channels were analysed using transfected CHO cells. Potassium currents were recorded at voltage sweeps from +60 mV to -120 mV (by -10 mV decrements) for 200 ms. Inward rectifying currents were inactivated in the presence of 1 mM BaCl_2 (Fig. 5A and B) and 10 mM BaCl_2 , respectively (Fig. 5D). The Ba^{2+} block of the inward current reversed readily upon washout (Fig. 5D).

Whereas 1 mM BaCl₂ did not affect the outward current at positive potential, 10 mM BaCl₂ led to the activation of cationic endogenous channels (Fig. 5C and D). Upon washout, this cationic current disappeared.

DISCUSSION

Potassium channels, including both Ca²⁺-activated and inwardly rectifying K⁺ channels, are the major class of ion channels involved in the generation of membrane potentials. The ability to control and regulate the resting membrane potential is due to an unusual conduction feature, which is now commonly referred to as inward and outward rectification. Such a definite electrical signature, perfectly characterized by conventional patch-clamp techniques, makes BK(Ca) and IRK channels attractive models for the validation of new planar patch-clamp chips. Large conductance calcium- and voltage-activated K⁺ channels are also referred to as “BK” (déjà dit) or “maxi-K” channels because of their high single channel conductance (250 – 300 pS), eliciting a large membrane current. The activation of BK channels leads to a small increase in extracellular K⁺ which shifts the reversal potential for K⁺ towards a more positive value. This leads to the activation of an IRK1 conductance of 23 to 30 pS, which is weaker than that of BK channels. In addition, both voltage-gated ion channels are targets for known drugs or divalent ions as well as potential targets for new biosensor approaches (Straub et al., 2001). For these reasons, efforts are being concentrated very much on understanding the properties of K⁺ channels as well as identifying new antagonists or activators (Busse et al., 1993, Nilius and Droogmans, 2001).

We have focused on optimising the coupling of the cells to planar chips in order to be able to record planar patch-clamps of resolved BK and IRK1 currents. We recorded ionic currents from BK(Ca) channels expressed in HEK-293 cells, as well as currents from IRK1 channels expressed in CHO cells, with known values of 250 pS and 30 pS, respectively. Current traces and current-voltage curves were similar to those obtained using conventional patch-clamping (data not shown). The capabilities of our

device for the detection of drug-induced modifications of ion channel functions were examined using iberiotoxin, a specific blocker of the BKs as well as Ba^{2+} , a divalent cation which is known to inhibit IRK1 currents. The onset and offset of the reversible Ba^{2+} block demonstrated the capacity of our device to introduce and remove compounds within seconds. In addition, Ba^{2+} is not only known to inhibit inward rectifying IRK1 currents but also to permeate through endogenous cationic channels at positive potentials. However this effect was not observed at a concentration of 1 mM, as was previously described in the literature (Skryma et al., 1994). With our device, Ba^{2+} permeation could only be observed at concentrations of 10 mM and higher.

It is generally agreed that the seal resistance value, the substrate surface state and the substrate (chip or pipette) capacitance are critical parameters in patch clamp experiments. We demonstrated that a 150 M Ω resistance seal, a 10 nm surface roughness and a 54 pF chip capacitance allowed ionic currents to be recorded in the whole-cell mode, permitting the pharmacological characterization of BK(Ca) and IRK1 channels.

Improving the frequency and quality of membrane sealing

Our experiments have shown that PECVD SiO_2 passivation leads to 155 M Ω – 7 G Ω seal resistances. Initially, we hypothesized that the reduction of aperture diameters from 2.5 μm to 1.7 μm , which is a value recently reported to be optimal for such applications (Pantoja et al., 2004), favoured the sealing process. However, similar results could not be obtained in experiments involving micro-structured chips using a mask of 1.7 μm diameter apertures (data not shown). This clearly indicates that aperture diameter is not the only factor which determines seal quality. Seal quality also depends on the length of membrane invagination in the microhole and the total contact surface. The optimal range of 1-2 μm holes should be a compromise between the surface offered by the microhole to the cell membrane and the elasticity of the cell membrane during aspiration. We assumed that PECVD SiO_2 deposition leads to larger sidewalls

and/or smoother angles of the microhole which provide a better contact area for seal formation (Sigworth and Klemic, 2002). The “hourglass” shape of the aperture, demonstrated by SEM observations, and the microhole resistance value, seem to favour formation and quality of the required seal. Rough edges were previously said to prevent adequate seal formation, so that care should be taken to obtain a clean and smooth surface around the microhole (Sigworth and Klemic, 2002, Corey and Stevens, 1983). For many, this apparently favours a good contact between the cell membrane and the substrate, only leaving a gap of a few Å (Corey and Stevens, 1983, Sakmann and Neher, 1984). While qualitative considerations have been advanced as “seal rules” or “seal recipe”, no scale or roughness values were given in most studies. However, our experiments showed that, despite the roughness caused by the PECVD SiO₂ layer the seal values were actually higher than those obtained on smooth, thermal SiO₂. It can therefore be assumed that an average roughness of 10 nm has a positive influence on the resistance value by increasing the contact area between the cell membrane and the substrate or that the sole physico-chemical properties of the SiO₂-coated surface improve seal quality. Future investigations will focus on determining the optimal degree of roughness, for example by modifying PECVD deposit parameters such as temperature or pressure, for optimal seal performances.

Device performances

Silicon introduces a capacitance due to the free charge carrier density of silicon (Fertig et al., 2003). This inherent high capacitance is the main drawback of silicon chips since electrical noise increases with capacitance (Wonderlin et al., 1990). The chips under investigation were initially coated with 2.12 µm thermal SiO₂ but the capacitance of 75 pF was too high to allow high resolution current recordings. The addition of an insulating layer of 1.5 µm SiO₂ PECVD reduced the chip capacitance from 75 to 54 pF. This range of capacitance must still be reduced further towards the values of 2 – 20 pF obtained with micropipettes. In a near future, we expect to decrease our capacitance to less than 10 pF by reducing the fluid contact surface and/or increasing the insulator layer. It is indeed desirable that the device capacitance

be no higher than the cell capacitance (10-100 pF) so that the cell membrane remains the dominant noise factor (Matthews and Judy, 2003).

The ability of a patch-clamp device to allow rapid and robust solution exchange with low sample solution consumption is one of the prerequisites for drug screening and ligand-gated channel analysis. The system under investigation allows the handling of small volumes in the analysis chambers of 4 μ l and is therefore suitable for drug screening applications. This was demonstrated by the block of BK(Ca) channels with 20 μ l of 100 nM iberiotoxin circulating in the microfluidics capillaries; traditional patch-clamp recordings usually require much larger volumes. Further optimizations are underway to decrease the compound volume to below 10 μ l.

This work constitutes a promising intermediary step showing whole-cell recordings and reversible detection of drug-induced modulation of ion channel activity. Using the multi-parametrical method described in this paper, we aim to produce new chips allowing a higher number of seals and higher seal resistance values. High resolution recordings and reduced reagents consumption open new application fields of the planar patch-clamp technology.

ACKNOWLEDGMENTS

We would like to thank Chris Lingle for providing the BK cDNA.

REFERENCES AND NOTES

- Asmild, M., Oswald, N., Krzywkowski, K. M., Friis, S., Jacobsen, R. B., Reuter, D., Taboryski, R., Kutchinsky, J., Vestergaard, R. K., Schroder, R. L., Sorensen, C. B., Bech, M., Korsgaard, M. P. and Willumsen, N. J. (2003) *Receptors Channels*, **9**, 49-58.
- Bruggemann, A., George, M., Klau, M., Beckler, M., Steindl, J., Behrends, J. C. and Fertig, N. (2003) *Assay Drug Dev Technol*, **1**, 665-673.
- Busse, R., Mülsch, A. and Fleming, I. (1993) *Circulation*, **87**, 18-25.
- Chien, K. (2003) *Nature Reviews Drug Discovery*, **3**, 239-278.
- Corey, D. P. and Stevens, C. F. (1983) *Eds. Bert Sakmann and Erwin Neher. Plenum Publishing Corp., New York.*, pp 53-68.
- Fertig, N., George, M., Klau, M., Meyer, C., Tilke, A., Sobotta, C., Blick, R. H. and Behrends, J. C. (2003) *Receptors Channels*, **9**, 29-40.
- Matthews, B. and Judy, J. W. (2003) *IEEE-EMBS International Conference on Neural Engineering*, 648-651.
- Mc Dowell, M. and Gray, E. (2004) *NASA/TM*, 1-8.
- Nilius, B. and Droogmans, G. (2001) *Physiol Rev*, **81**, 1415-59.
- Owen, D. and Silverthorne, A. (2002) *drug discovery world*, **3**, 48-61.

Pantoja, R., Nagarah, J. M., Starace, D. M., Melosh, N. A., Blunck, R., Bezanilla, F. and Heath, J. R.

(2004) *Biosens Bioelectron*, **20**, 509-17.

Picollet-D'Hahan, N., Sordel, T., Garnier-Raveaud, S., Sauter, F., Ricoul, F., Pudda, C., Marcel, F. and

Chatelain, F. (2004) *Sensor letters*, **2**, 91-94.

Sakmann, B. and Neher, E. (1984) *Annu Rev Physiol*, **46**, 455-72.

Seo, J., Ionescu-Zanetti, C., Diamond, J., Lal, R. and Lee, L. P. (2004) *Applied physics letters*, **84**, 1973-

1975.

Sigworth, F. J. and Klemic, K. G. (2002) *Biophys J*, **82**, 2831-2832.

Skryma, R., Prevarskaya, N., Vacher, P. and Dufy, B. (1994) *FEBS Lett*, **349**, 289-294.

Stett, A., Bucher, V., Burkhardt, C., Weber, U. and Nisch, W. (2003a) *Med Biol Eng Comput*, **41**, 233-

240.

Stett, A., Burkhardt, C., Weber, U., van Stiphout, P. and Knott, T. (2003b) *Receptors Channels*, **9**, 59-66.

Straub, B., Meyer, E. and Fromherz, P. (2001) *Nat Biotechnol*, **19**, 121-4.

Tao, H., Guia, A., Sithiphong, K., Miu, P., Ligutti, J., Wu, L. and Xu, J. (2004).

Venter, J. C., Adams, M. D., Myers, E. W., Li, P. W., Mural, R. J., Sutton, G. G., Smith, H. O., Yandell,

M., Evans, C. A., Holt, R. A., Gocayne, J. D., Amanatides, P., Ballew, R. M., Huson, D. H., Wortman, J.

R., Zhang, Q., Kodira, C. D., Zheng, X. H., Chen, L., Skupski, M., Subramanian, G., Thomas, P. D.,

Zhang, J., Gabor Miklos, G. L., Nelson, C., Broder, S., Clark, A. G., Nadeau, J., McKusick, V. A., Zinder, N., Levine, A. J., Roberts, R. J., Simon, M., Slayman, C., Hunkapiller, M., Bolanos, R., Delcher, A., Dew, I., Fasulo, D., Flanigan, M., Florea, L., Halpern, A., Hannenhalli, S., Kravitz, S., Levy, S., Mobarry, C., Reinert, K., Remington, K., Abu-Threideh, J., Beasley, E., Biddick, K., Bonazzi, V., Brandon, R., Cargill, M., Chandramouliswaran, I., Charlab, R., Chaturvedi, K., Deng, Z., Di Francesco, V., Dunn, P., Eilbeck, K., Evangelista, C., Gabrielian, A. E., Gan, W., Ge, W., Gong, F., Gu, Z., Guan, P., Heiman, T. J., Higgins, M. E., Ji, R. R., Ke, Z., Ketchum, K. A., Lai, Z., Lei, Y., Li, Z., Li, J., Liang, Y., Lin, X., Lu, F., Merkulov, G. V., Milshina, N., Moore, H. M., Naik, A. K., Narayan, V. A., Neelam, B., Nusskern, D., Rusch, D. B., Salzberg, S., Shao, W., Shue, B., Sun, J., Wang, Z., Wang, A., Wang, X., Wang, J., Wei, M., Wides, R., Xiao, C., Yan, C., et al. (2001) *Science*, **291**, 1304-1351.

Wang, X. and Li, M. (2003) *Assay Drug Dev Technol*, **1**, 695-708.

Wonderlin, W. F., French, R. J. and Arispe, N. J. (1990) In *Neuromethods: Neurophysiological Techniques: Basic Methods and Concepts*, Vol. 14 (Eds, Boulton, A. A., Baker, G. B. and Vanderwolf, C. H.) The Humana Press Inc., Clifton, pp. 35-142.

Wood, C., Williams, C. and Waldron, G. J. (2004) *drug discovery today*, **9**, 434-441.

Xu, J., Chen, Y. and Li, M. (2004) *drug discovery today*, **3**, 32-38.

Xu, J., Guia, A., Rothwarf, D., Huang, M., Sithiphong, K., Ouang, J., Tao, G., Wang, X. and Wu, L.

(2003) *Assay Drug Dev Technol*, **1**, 675-684.

Table 1: Effect of SiO₂ PECVD deposition on typical electrical characteristics of chips.

Three different PECVD SiO₂ thicknesses (e_d) were investigated: 0.5, 1 and 1.5 μm . Microhole diameter (\varnothing_d) measured with SEM, theoretical (th) and experimental (exp) microhole resistance (R_h) and cell-patch site capacitance (C) are reported for each type of PECVD deposit. Resistance was calculated according to equations 1 and 2 using model 2 (see text) and capacitance according to Eq. 3 and 4 (see text). A good correlation of resistance and capacitance with the thickness of PECVD SiO₂ layers was observed. (*): *no measurement performed*.

SiO ₂ e_d thickness (μm)	\varnothing_d μhole (μm)	Microhole resistance (R_h , $\text{M}\Omega$)		Capacitance (C, pF)	
		R_h (th)	R_h (exp)	C (th)	C (exp)
0	2.50	0.46	0.55	70	75
0.5	2.20	0.62	0.65	62	- (*)
1.0	1.95	0.87	0.85	58	- (*)
1.5	1.70	1.24	1.15	51	54

Figure legends

Figure 1: Cell-patch site made of thermal SiO₂ (left column) and PECVD SiO₂ (right column).

Microhole diameter determination on scanning electron (SE) micrographs before (A) and after (B) passivation (1.5 μm thick SiO₂ layer). Surface roughness visualization on AFM pictures before (C) and after (D) passivation of the same chips. The four squares on both images represent the roughness calculation areas. The arrow indicates a 112 nm high asperity. Topography curves along the horizontal black axis of Fig. 1, C and D for microholes before (E) and after (F) PECVD deposition. From these curves, the flatness around the microhole has been quantified (see text).

Figure 2: Schematic cross section representation of silicon chip capacitance (not scaled) and modelled cell-patch-site resistance and measurements.

Top view A: two capacitors are formed by the conducting parallel plates of electrophysiological medium (*zones A and D*) and the silicon substrate (*zone C*) separated by the SiO₂ dielectric layer (*zones B₁ and B₂*). B₁ represents the PECVD SiO₂ layer and B₂ the thermal SiO₂ layer. Views B and C: enlarged view of the microhole depicting the aperture shape following the deposition process modeled by model 1 (view B) and model 2 (view C) ($e_0 = 2.12 \mu\text{m}$, $\varnothing_0 = 2.5 \mu\text{m}$, e_d is the PECVD SiO₂ thickness and \varnothing_d the microhole diameter after deposition). Bottom view D: three SiO₂ thicknesses are reported with corresponding experimental and theoretical microhole resistance values. The curve (■) presents resistance values theoretically evaluated with model 1 (see text) and the curve (Δ) presents those evaluated with model 2. Experimental results (on n=5) are reported on curve (♦). A good correlation between experimental resistance and theoretical resistance values according to model 2 was observed.

Figure 3: Distribution of seal resistances.

Distribution of seal resistances higher than 100 MΩ obtained on chips with SiO₂ PECVD layer.

Figure 4: Whole cell K⁺ currents recorded from BK(Ca) channels with the chip device.

Current recordings were performed in the whole-cell configuration from HEK cells expressing BK-type Ca²⁺-activated channels. **A:** outward rectifying potassium currents elicited with activating voltage steps from a holding potential of 0 mV to + 120 mV with 10 mV increments. Seal resistance: 150 MΩ. Whole-cell measurements demonstrating the specific inhibitor effect of the scorpion peptide toxin iberiotoxin (IBTX) on BK(Ca) channels. Outward K⁺ currents were significantly reduced by 100 nM IBTX. **B:** Current tension relation curve obtained from previous current traces (seal leak current was subtracted).

Figure 5: Whole cell K⁺ currents recorded from IRK1 channels with the chip device.

Current recordings were performed in the whole-cell configuration from CHO cells expressing IRK1 channels. **A:** inward rectifying potassium currents elicited with activating voltage steps from 0 mV to -120 mV with 10 mV decrements. Seal resistance: 100 MΩ. Blocking effect on inward K⁺ currents of the unspecific Ba²⁺ divalent (1 mM). The capacitive peaks are related to the planar structure of the silicon chip. Typical data are displayed without applying leak subtraction. **B:** Current tension relation curve obtained from previous current traces (no leak compensation). **C:** activation of endogenous Ca²⁺ channels by 10 mM BaCl₂ with activating voltage steps from 0 to +60 mV (P/4 leak subtraction was displayed). **D:** Inward rectifying K⁺ currents were elicited by a voltage pulse from +60 to -90 mV (□) and were inhibited in the presence of 10 mM BaCl₂ (■). The part of the curve (■) at positive potentials shows the activation of endogenous Ca²⁺ channels by 10 mM BaCl₂. The I-V curve (x) was plotted after blocker washout and shows the reversible effect of BaCl₂. P/4 leak subtraction was displayed.

Figure 1

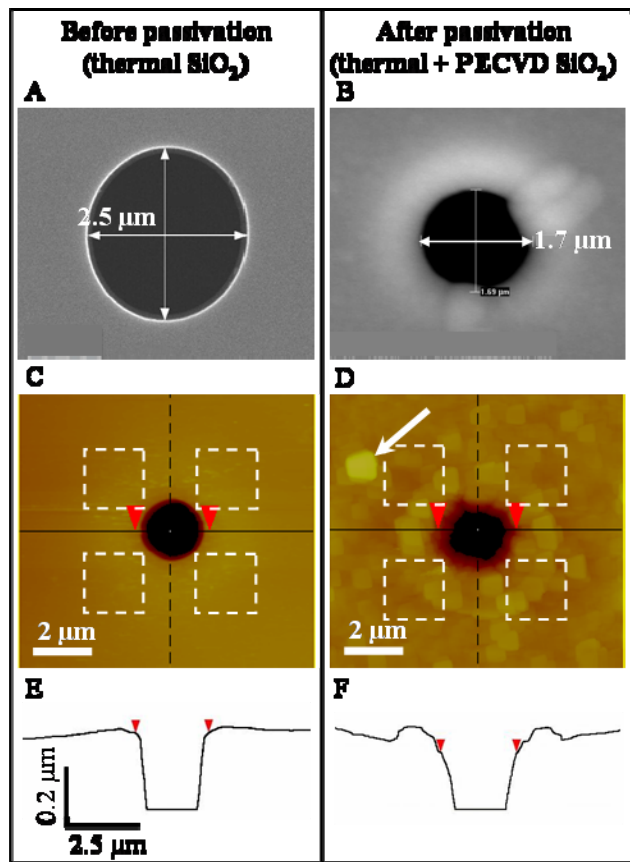


Figure 2

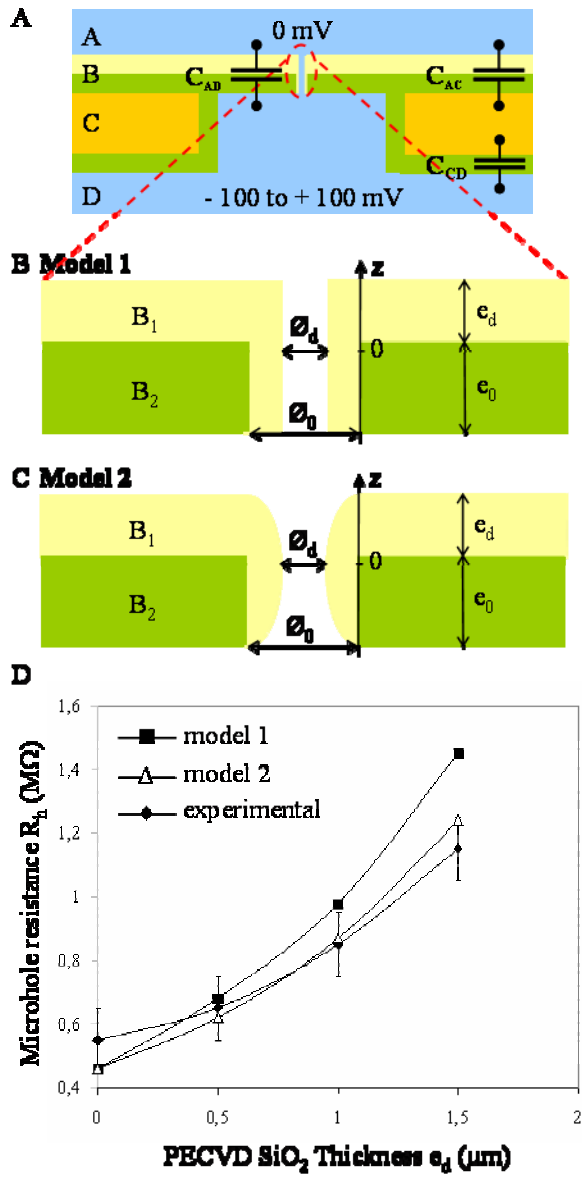


Figure 3

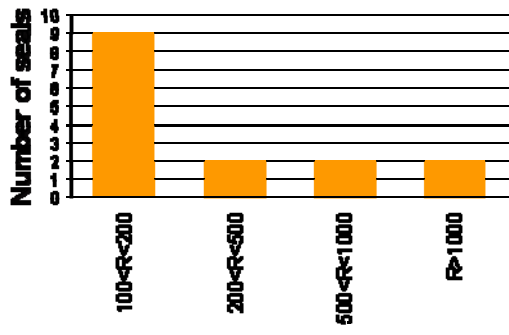


Figure 4

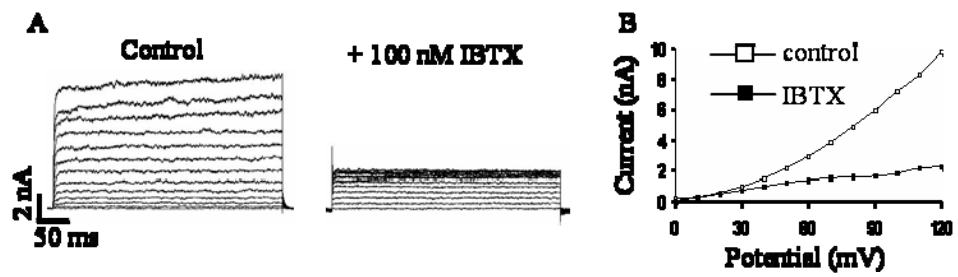


Figure 5:

